Scaling Laws for Lennard-Jones Bead-Spring Polymers with Coulombic Charges

Isaac Zakaria

13 December 2019

Abstract

Lennard-Jones (LJ) bead-spring polymers with screened Coulomb interactions provide an illustrative coarse-grained system for probing scaling laws in biopolymers. Here, I use molecular dynamics to simulate LJ polymers with alternating positively and negatively charged monomers at a variety of chain lengths and charge screenings to show how the diffusion, energetics, and configurations of polymers are affected by the strength of Coulomb interactions. Lower charge screening tends to depress the diffusion coefficient across all chain lengths. The energies of charged polymers tend to fluctuate more at longer chain lengths and with stronger Coulomb interactions. The more stable energetics of shorter chains can be explained by the increase in average coordination number at charged sites at lower degrees of polymerization. There appears to be a plateau in coordination number for longer chain lengths; this is likely a configurational effect that results due to constraints imposed by bonded interactions—the same effect that reduces the diffusion coefficient for longer chains.

1. Introduction

Charged biopolymers are used by animals to produce iridescent camouflage. For instance, the reflectin A1 protein is believed to be used by the squid *Doryteuthis opalescens* to change the refractive index of its skin. Recent work by the Gordon group aims to describe the electrochemical properties of reflectins that govern their self-assembly into aggregates of nearly uniform diameter. This aggregation, driven by changes in electrochemical parameters such as electrolyte concentration or applied charge, is hypothesized to be the underlying process that enables *Doryteuthis opalescens* achieve controllable iridescence.

In this study, systems of Lennard-Jones (LJ) bead-spring polymers with alternating positive and negative charges at regular intervals were simulated to mimic the qualitative behavior of charged biopolymers in aqueous electrolytic solutions. Molecular dynamics (MD) simulations were employed to probe how the diffusion coefficient, energetics, and average coordination numbers of charged LJ polymers vary at different degrees of polymerization ($M = 3,6,12,$ and 15) and charge screening ($\lambda_D^* = 0,5,10,15,20,30,40,50,75$ and 100).

2. Methods

2.1. Charged LJ Polymer Model

LJ polymers were constructed by repeating the 6-bead motif illustrated in Figure 1.

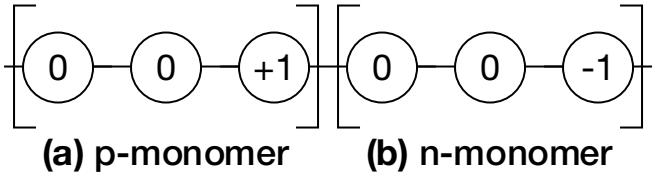

Figure 1: 6-bead motif used to construct the LJ polymers of interest, separated into 2 monomers: **(a)** a p-monomer and **(b)** an n-monomer.

The motif is sub-divided into a positive (p) and negative (n) monomer, both of which contain 3 beads. For odd values of M, 2 types of polymers result: a positive type with $M/2+1$ p-monomers alternating with $M/2-1$ n-monomers with p-monomers at the head and tail, and an analogous negative type with $M/2+1$ n-monomers that starts and terminates with n-monomers. When $M=3$, the simulated system is a binary mixture of unbonded p- and n-monomers. For even M, the polymers are all identical.

2.2. Governing Potential and Force Field

Charged LJ polymers were simulated in an implicit electrolytic solution with screened Coulomb interactions using the potential in Equation 1. For simplicity, reduced units were used, leading to the definitions in Table 1. The charge (q_i) of a given particle i takes on a value of zero or ± 1; consequently, the non-bonded interaction simplifies to a pure-LJ interaction if one or both particles are not charged (*i.e.* when q_i or q_j is zero).

$$U^*(\mathbf{r}^N) = \sum_{i<j,\text{non-bonded}} \left[4\left(\frac{1}{r_{ij}^{*12}} - \frac{1}{r_{ij}^{*6}} \right) + \epsilon_C \frac{q_i q_j}{r_{ij}^*} \exp\left(-\frac{r_{ij}^*}{\lambda_D^*} \right) \right] + \sum_{i<j,\text{bonded}} k^* \frac{\left(r_{ij}^* - r_0^*\right)^2}{2} \quad (1)$$

Table 1: Definitions of potential energy parameters alongside dimensionless equivalents. ε and σ are the LJ well depth and characteristic inter-particle distance. q_e is the elementary charge, ϵ_0 the permittivity of free space, and ϵ_S the permittivity of the solvent.

Parameter	Dimensional Form	Dimensionless Equivalent
Potential energy	U	$U^* \equiv \frac{U}{\varepsilon}$
Pairwise distance	r_{ij}	$r_{ij}^* \equiv \frac{r_{ij}}{\sigma}$
Debye length	λ_D	$\lambda_D^* = \frac{\lambda_D}{\sigma}$
Coulomb potential constant	$\frac{q_e}{4\pi\epsilon_0\epsilon_S}$	$\epsilon_C = \frac{q_e}{4\pi\epsilon_0\epsilon_S\sigma\varepsilon}$
Equilibrium bond distance	r_0	$r_0^* = \frac{r_0}{\sigma}$
Harmonic spring constant	k	$k^* = \frac{k\sigma}{\varepsilon}$

The Debye length (λ_D) is empirically observed to be proportional to the inverse-square of the electrolyte concentration; longer Debye lengths correspond to lower electrolyte concentrations, and thus a lower degree of charge screening and stronger Coulomb interactions.

The pairwise force in reduced units is given by Equation 2, where $\widehat{\mathbf{r}_{ij}}$ is the unit vector in the direction of the dimensionless pairwise distance ($\mathbf{r}_{ij}^*$).

$$\mathbf{f}_{ij}^{*}(\mathbf{r}_{ij}^{*}) = \begin{cases} \left[\left(-\frac{48}{r_{ij}^{*\,13}} + \frac{24}{r_{ij}^{*\,7}}\right) + \epsilon_C \frac{q_i q_j}{r_{ij}^{*}}\left(\frac{1}{r_{ij}^{*}} - \frac{1}{\lambda_D}\right)\exp\left(-\frac{r_{ij}^{*}}{\lambda_D}\right)\right]\widehat{\mathbf{r}_{ij}}, & i,j \text{ not bonded} \\ k^{*}\left(r_{ij}^{*} - r_0^{*}\right)\widehat{\mathbf{r}_{ij}}, & i,j \text{ bonded} \end{cases} \quad (2)$$

2.3. Simulation Parameters

All MD simulations were conducted with $N = 300$ beads (150 positive and 150 negative) in the canonical ensemble within a square simulation box under periodic boundary conditions. The length of the box was selected to achieve a number density of $\rho = 0.8$. Velocity rescaling was applied to target a temperature of $T = 1.0$. This temperature and density were selected because a LJ bead system with no Coulomb or bonded interactions is liquid under these conditions. All simulations were equilibrated for 50,000 time steps, during which velocities were rescaled every 50 timesteps; all production run simulations were 200,000 timesteps. Error bars on computed quantities were obtained by rerunning each simulation in triplicate with different starting configurations and averaging the results. The parameters in Equations 1 and 2 were chosen at $k^{*} = 3{,}000$, $r_0^{*} = 1$, and $\epsilon_C = 10$. Simulations with a Debye length of zero were carried out by setting $\epsilon_C = 0$. The non-bonded potential was truncated at a cutoff radius of 2.5 with an appropriate shift applied. Diffusion coefficients (D) were calculated from mean-squared displacement timeseries data (MSD) via Equation 3. Average coordination numbers were computed within a radius of 1.5.

$$D = \frac{1}{6} \times (\text{MSD timeseries linear regression slope}) \quad (3)$$

3. Results and Discussion

Trends in the diffusion coefficients (Figure 2) suggest that Coulomb interactions tend to dominate the mobility of the charged polymers. At each degree of polymerization, D quickly approaches an asymptotic value after $\lambda_D^{*} \approx 10$. Over the range of charge screenings simulated, the diffusion coefficients across different degrees of polymerization remained within an order of magnitude of one another.

Figure 3 reveals that the absolute value of the relative standard deviation of U^{*}, $\left|\sigma_{U^{*}}\langle U^{*}\rangle^{-1}\right|$, generally experiences greater fluctuations with Coulomb interactions than without. $M = 3$ appears to be relatively immune to this trend: at this degree of polymerization, the fluctuations in $\left|\sigma_{U^{*}}\langle U^{*}\rangle^{-1}\right|$ are much smaller and are more consistent across different charge screenings.

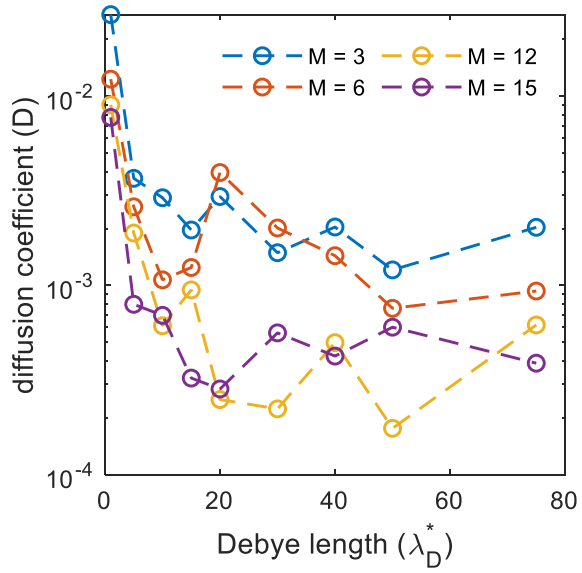

Figure 2: Diffusion coefficient at each M, scaled logarithmically.

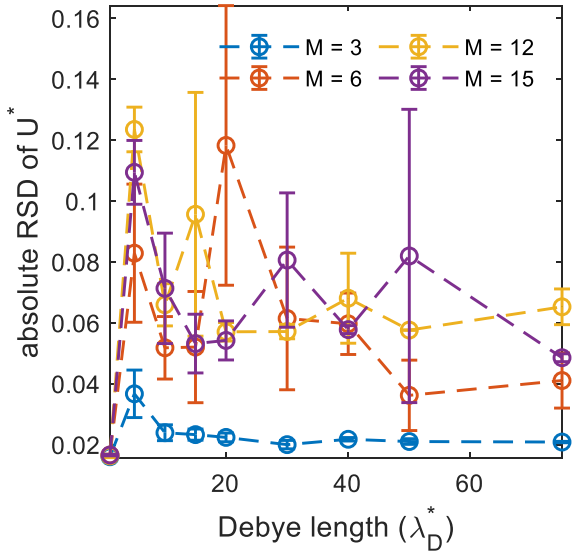

Figure 3: The absolute relative standard deviation (RSD) of U^*, $|\sigma_{U^*}\langle U^*\rangle^{-1}|$ at each M.

The trends in the average coordination number (Figure 4) provide insight into why chains with $M = 3$ exhibit smaller fluctuations in potential energy. The average coordination number for all atoms (Figure 4a) increases when Coulomb interactions are added. Figure 4c demonstrates that, for a fixed Debye length, the average coordination number at charged sites tends to increase for shorter chains; this effect appears to drive the change in average coordination number observed in Figure 4a. Higher coordination results in greater charge stabilization, and by extension, a higher degree of energetic stability. The average coordination number for $M = 3$ at all sites is lower than that for longer chains because single-monomer chains are more mobile—and hence can achieve configurations with greater charge stabilization. The average coordination number at charged sites appears to plateau after $M = 12$; after this point, chain configuration is highly limited by the constraints imposed by bonded interactions. The average coordination number for neutral sites (Figure 4b) increases at longer Debye lengths for $M \geq 6$ because Coulomb interactions tend to bring neighboring chains closer together; by contrast, when $M = 3$, the average coordination at neutral sites decreases because the chains configure themselves to prioritize interactions between charged sites for charge stabilization.

4. Conclusion

Simulations at varied chain lengths and charge screenings show that Coulomb effects dominate the diffusive and configurational properties of simple charged polymers. Diffusion slows down as Coulomb interactions become stronger and energetics become less stable—though, intuitively, a decreasing trend in the diffusion coefficient for longer chains is still observed. The average

coordination number at charged sites suggests that these Coulomb-dominated effects are the result of preferential configurations driven by a tendency toward charge stabilization. In longer chains, these charge-stabilizing configurations are limited by bonded interactions.

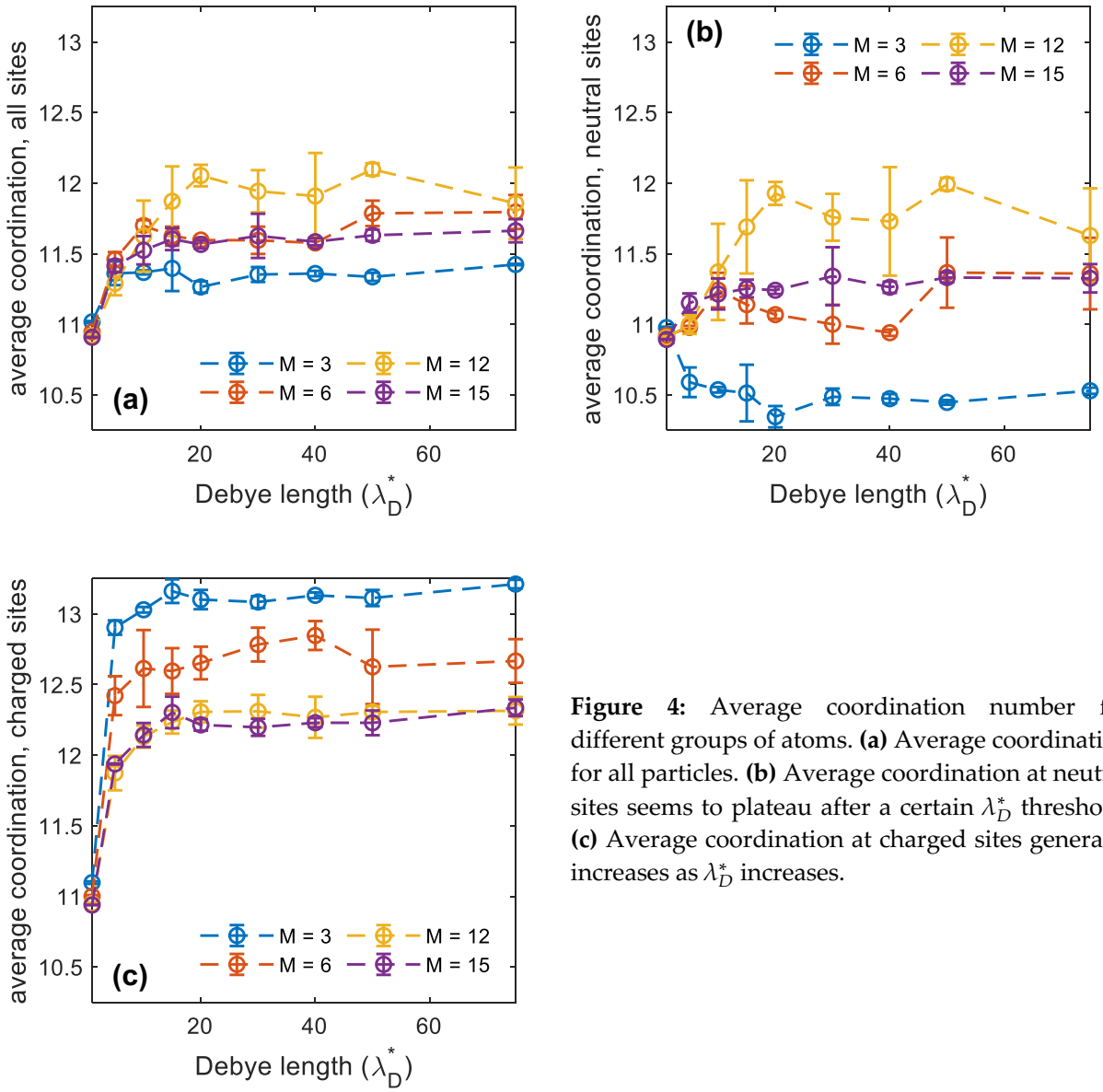

Figure 4: Average coordination number for different groups of atoms. **(a)** Average coordination for all particles. **(b)** Average coordination at neutral sites seems to plateau after a certain λ_D^* threshold. **(c)** Average coordination at charged sites generally increases as λ_D^* increases.

To further probe the sensitivity of these trends to charge screening, it may be illustrative to conduct more simulations in the highly-screened regime, where the Debye length is very close to zero. In addition, by applying Ewald summation, the unscreened case may also be investigated. Finally, these property simulations may be applied to polyatomic systems with different magnitudes of charge at different sites and different Lennard Jones radii—for instance, systems in which each bead has the average charge properties of an amino acid residue at a fixed pH—to more accurately approximate the behavior of biopolymers.

Movie

The included movie, `IZakaria_210D_movie_M12.mp4`, visualizes 20,000 timesteps (400 frames) of the MD simulation for $N = 300$, $M = 12$, and $\lambda_D^* = 100$ with a single chain highlighted and positive and negative charges indicated. Figure 5 displays a still from this movie (the simulation box has been rotated to improve visibility of the highlighted chain). For clarity, the radius of the of atoms illustrated in the simulation is 50% of the actual atomic radius. Segments of the chain appear in different parts of the box due to periodic boundary conditions.

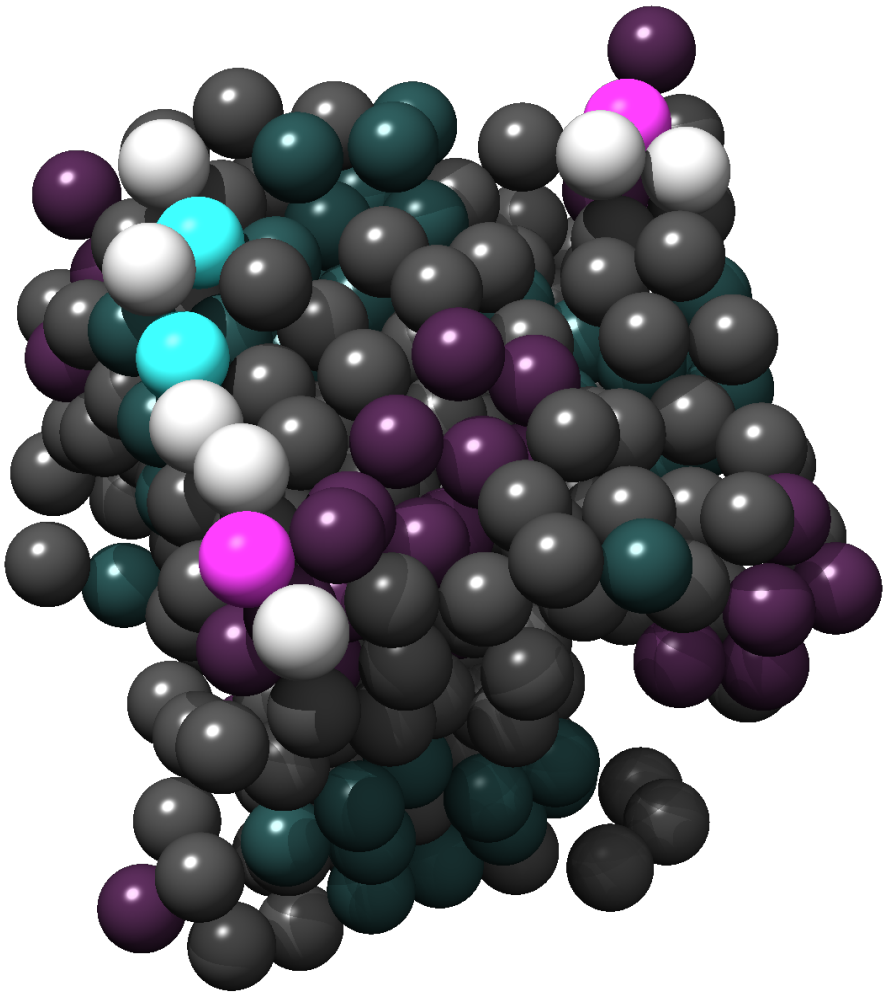

Figure 5: Still captured from `IZakaria_210D_movie_M12.mp4`. $N = 300$, $M = 12$, and $\lambda_D^* = 100$. Light atoms (white, magenta, and cyan) highlight a single chain. Gray atoms are neutral, magenta atoms are positive, and cyan atoms are negative.